Effect of Hole Space Ratio on Effusion Cooling Performance

Dr. Khalid Faisal Sultan

University of Technology, Baghdad, Iraq

Abstract

The film cooling effectiveness and local heat transfer coefficient for different hole space ratio have been experimentally investigated on a flat plate in the current study. The investigations were done by using a single test transient IR thermography technique. Three models of staggered holes arrangement are investigated.). Each model is provided with five columns of holes, these models are arranged with staggered row holes. The holes diameter is 4mm, the longitudinal distance (X/D) is 10, and the span distance between two neighboring holes (S/D) are 3, 5, and 7 respectively. The attitude of the holes is fixed at inclination angle ($\theta = 30^o$). The blowing ratios, cold to hot air flow ratio, have been changed three times (BR= 0.5, 1.0, and 1.5) during the experimental program. The experimental investigation showed that the thermal performance decreases as the space ratio (S/D) increases for all blowing ratios, and the film cooling effectiveness decreases as the blowing ratio increases for all the three models.

تأثير نسبة المسافة الجانبية للفتحات على اداء تبريد الانتشار

في هذه الدراسة تم حساب فعالية غشاء التبريد ومعامل أنتقال الحرارة، حيث أجريت تجارب عملية لفتحات نفث مختلفة المسافات الجانبية على صفيحة مستوية وذلك بأستخدام تقنية الصورة الحرارية تحت الحمراء (IR) بالية الفحص الأنتقالي الواحد. لقد تم فحص ثلاث نماذج من الفتحات المتعرجة (staggered) الترتيب، وكل نموذج مزود بخمسة أعمدة من الفتحات الدائرية. تم تثبيت قطر الفتحات (D) بمقدار (4 mm) والمسافة الطولية بين صف وأخر (X/D) بمقدار (10) ، بينما تم أخذ المسافة بين الفتحات المتجاورة (S) في الصف الواحد بالمسافات 3، 5، و 7 على التوالي، وكذلك تم تثبيت زاوية ميل الفتحات بمقدار (30^o). كما تم دراسة تأثير نسبة نفخ الهواء البارد الى الحار (BR) بالنسب 0.5، 1.0، و 1.5.

النتائج العملية بينت أن أداء التبريد يقل بزيادة نسبة المسافة الجانبية لجميع نسب النفخ المدروسة، و أن فعالية غشاء التبريد تقل مع زيادة نسب النفخ.

1- Introduction

Modern gas turbine engines are designed to perform at high inlet temperature of (1800-2000 ºK) to improve thermal efficiency and power output. As the turbine inlet temperature increases, the heat transferred to the blades in the turbine also increases. Since this temperature exceeds the melting point of the turbine blade materials of about (≈ 1480 K). Therefore, there is a need for an efficient cooling system engineered in away such that the maximum blade surface temperature during operation is well below the maximum melting point of the blade material. To achieve that, researchers focus on various innovative cooling techniques depending on the nature of the coolant flow [1].

Film cooling primarily depends on the coolant-to-mainstream pressure ratio or can be related to the blowing ratio, temperature ratio (T_c/T_m), and the film cooling hole location, configuration and distribution on a turbine elements film cooling. In a typical gas turbine blade, the range of the blowing ratios are of about approximately between 0.5 and 2.0, while the (Tc/Tm) values vary between 0.5 and 0.85 Han and Ekkad [2].

Effusion (or transpiration) cooling, which contains an array of closely spaced discrete film cooling holes, is widely used to cool and insulate the component metal from the hot mainstream flow. The cooling effectiveness of an effusion cooling plate depend on several parameters, such as hole spacing, angle, diameter, etc.

Review on turbine cooling technology developments has been well described by Han et al. [3] and Bunker [4] which covering of all the available technologies on film cooling. Ahn et al. [5] presented the injectant behavior from two rows of film cooling holes with opposite orientation angles. Four film cooling hole arrangements were considered including inline and staggered ones. Detailed adiabatic film cooling effectiveness distributions were also measured using Thermochromic Liquid Crystal (TLC) to investigate how well the injectant covers the film cooled surface. Later. Han and Rallabandi [6] stated that the pressure sensitive paint technique proved very high resolution contours of film cooling effectiveness, without being subjected to the conduction error in high thermal gradient regions near the hole. Andrews et al. [7] investigated (90 deg.) cooling hole for a number of different arrays and found that there was a significant improvement in the overall cooling effectiveness for a larger hole relative to a smaller hole. Andrews et al. [8] also compared normal (90 deg.) and inclined film holes (30 deg. and 150 deg.) for an array of effusion holes and found that cooling effectiveness improved with inclined holes. The counter flow holes (150 deg.) resulted in reverse flow and good cooling performance at low coolant flows but not at high coolant flows.

Lu et al. [9 and 10] presented the experimental and numerical investigation of film cooling performance for a row of cylindrical holes in modern turbine blade. The adiabatic film effectiveness and heat transfer coefficient are determined experimentally on a flat plate downstream of a row of inclined different geometries hole exit by using a single test transient IR thermograph technique at four different coolant-to-mainstream blowing ratios of 0.5, 1.0, 1.5 and 2.0. Four test designs crescent and converging slot, trench and cratered hole exits, are tested. Results showed that both the crescent and slot exits reduce the jet momentum at exit and also provide significantly higher film effectiveness with some increases in heat transfer coefficients.

Martiny et al. [11] used a very low injection angle of (17 deg.) for an effusion, film cooling plate in which they measured adiabatic effectiveness levels for a range of blowing ratios. Their results indicated significantly different flow patterns depending on the cooling jet blowing ratio. It is important to recognize that their study used only four rows of cooling holes and as will be shown in this paper, this small number of rows did not allows for a fully developed condition to occur.

Gustafsson and Johansson [12] investigated the temperature ratios and velocity ratios between hot gas and coolant, and different injection hole spacing, inclination angle, and thermal conductivity of the test plate.

Ekkad et al. [13] obtained both film cooling effectiveness and heat transfer coefficient from a single test by means of the transient infrared thermography technique. The advantage of IR technique was exhibited adequately in these previous research efforts. In terms of the wider temperature range handled than the liquid crystal technique and more detailed 2D temperature field information with better accuracy. It is seen that these research with successful employed of the IR technique enriched higher quality data in the literature, but the effect of the deflection angle of the injection holes was not attempted.

Dhungel et al. [14] obtained simultaneously detailed heat transfer coefficient and film effectiveness measurements using a single test transient IR thermography technique for a row of cylindrical film cooling holes, shaped holes. A number of anti-vortex film cooling designs that incorporate side holes. They found that the presence of anti-vortex holes mitigates the effect of the pair of anti-vortices.

Numerical prediction of Alwan [15] showed that the flow field structure of injected holes present vortices, such as counter pair kidney vortex and horseshoe vortex have major effects on cooling performance, in which the strength of the kidney vortex decreases and the horseshow vortex is lifting up, leading to an improvement in the coolant performance.

Therefore, numerical model is suitable to design holes arrangement futures of film cooling system by introducing oriented holes row over single jet holes row.

At the present work, experimental investigations were done to evaluate the film cooling performance for different hole space ratio and different blowing ratio in order to determine the heat transfer coefficient and the film cooling effectiveness on a flat plate by using a single test transient IR thermograph technique.

2- Experimental Facilities

A schematic diagram and photography of the low speed open duct jet test rig is shown in figure 1 was used at the current investigation. The mainstream air supply is the ambient air drawn by a centrifugal backward blade blower. The blower is driven by 2.5 kW motor running with 2800 rpm. Manual open gate is used to control the air speed in the tunnel test section. The blower exit area having rectangular shape with dimensions of (6.3x13.1) cm. The blower is supplied with bend having the same dimensions of the blower exist and then connected to a diffuser having rectangular cross-section area of inlet and outlet dimensions as (6.3x13.1) cm and (35x50) cm respectively and length of (82) cm. Air flow diffuses over a splitter plates into a constant area rectangular settling chamber of cross-section area (35x50) cm and length of 70 cm. The settling chamber contains a series of three electrical heaters each of 4 kW power and four grid screen. This ensures adequate mixing of hot air and uniform temperature distribution throughout the test section. Then the hot air routed through a convergent- divergent contraction having a rectangular cross-section area from (35x50) cm to (5x10) cm and length of 70 cm. In order to allow the air to reach the desired temperature, the air is initially routed out away from the test section by using a by-bass gate passage. The temperature of the air is continuously monitored at the exit of the gate and when the desired temperature is reached, the gate is fully opened manually and air flow passes into a test section through a rectangular duct area. To minimize the heat losses to the surrounding the settling chamber and the test section duct are insulated completely. The operating velocity of the hot air in the test section is controlled to run from 20 to 40m/s through the experimental program. The test section has 50mm width and 100mm height. The bottom plate of the test section is made of (234x123) mm Plexiglas of 10mm thickness.

A centrifugal air blower of blowing capacity of (22.17) m^3/min was used to supply the coolant air to the plenum. The plenum was located below the test plate. The coolant air enters a plenum then ejected through holes into the test section. The coolant air pressure measured at the inlet of the test section. The coolant air injected from the holes is mixed with the hot

mainstream in the test section. The test section has 5 cm width, 10 cm height and 23.4 cm length. The bottom wall of the test section work as a test model, three models with different hole pitch ratio are prepared, The bottom model plate can be removed easily to be replaced by another model at each test. Each model is provided with five columns of holes, these models are arranged with staggered row holes. The holes diameter is 4mm, the longitudinal distance (X/D) is 10, and the span distance between two neighboring holes (S/D) are 3, 5, and 7 respectively. The attitude of the holes is fixed at inclination angle ($\theta = 30^{o}$), where the inclination angle (θ) is defined as the angle between the centerline of the hole and the surface of the test wall.

The surface temperature of test model was measured using an infrared thermographs technique. IR thermograph infrared camera type Fluke Ti32 was used in the present investigation. This camera is able to precisely record the temperature variations. The IR system is greatly affected by both background temperature and local emissivity. The test surface is sprayed with mat black color to increase the emissivity like a perfect black body. The temperature measurement taken is not accurately recorded unless the IR system is calibrated.

The system was calibrated by measuring the temperature of the test surface using thermocouple type K and the reading of IR camera. The test surface is heated by mainstream hot air. The measured temperatures obtained by both ways are recorded and stored during the heating process until achieving a steady state condition. Due to the emissivity of the test surface, the temperature obtained by IR camera is different from the temperature obtained by the thermocouple. Therefore, the IR camera reading is adjusted until both temperature readings are matched.

The IR images taken for the test surfaces at each test are stored in the SD memory of IR camera. These images are transferred from SD memory to PC memory. Then the middle region of the test surface area is then selected to eliminate the effect of the test section wall with using camera software, Smart View Software Program. IR images, which exhibit the temperatures distribution as colors code, is converted to corresponding temperature digit values by using Smart View Software and then saved as output data in Excel sheet.

2-1- Procedure

Consider the transient flow over a flat plate. In this case, the test plate is initially at a uniform temperature T_i, and the convective boundary condition is suddenly applied on the plate at time t > 0. Now, the heat is assumed to be conducted only in the x-direction and perform an energy balance on the plate. Therefore the one-dimensional transient conduction equation is

$$\frac{\partial^2 T}{\partial x^2} = \frac{1}{\alpha}\frac{\partial T}{\partial t} \qquad (1)$$

The main approximation often applied to analyze transient conduction shown in Figure 4 is the semi-infinite approximation. The semi-infinite solid assumptions are valid for the present investigation for two reasons. Firstly, the test duration is small, usually less than 60 seconds. Secondly, the hot air flows over the test surface is made from Plexiglas of, low thermal conductivity, low thermal diffusivity, and low lateral conduction. Therefore, the solution of equation (1), as given by Holman and Bhattacharyya [16], is as follows:

$$\frac{T_w - T_i}{T_m - T_i} = 1 - \exp\left[\frac{h^2 \alpha t}{k^2}\right] erfc\left[\frac{h\sqrt{\alpha t}}{k}\right] \qquad (2)$$

Where T_w measured by using IR camera, all the other variables in the equation (2) are either known variables or measured variables except the heat transfer coefficient (h).

In the film cooling case, the film should be treated as a mixture of air mainstream and the coolant air, the mainstream temperature (T_m) in equation(2) has to be replaced by the film temperature (T_f).Therefore, equation (2) becomes as:

$$\frac{T_w - T_i}{T_f - T_i} = 1 - exp\left[\frac{h^2 \alpha t}{k^2}\right] erfc\left[\frac{h\sqrt{\alpha t}}{k}\right] \qquad (3)$$

A non-dimensional temperature term is known as the film cooling effectiveness (η), and is defined as:

$$\eta = \frac{T_f - T_m}{T_c - T_m} \qquad (4)$$

Equation (3) has two unknowns (h and T_f).To solve this equation, two sets of data points are required to obtain the unknowns like:

$$\frac{T_{w1} - T_i}{T_f - T_i} = 1 - exp\left[\frac{h^2 \alpha t_1}{k^2}\right] erfc\left[\frac{h\sqrt{\alpha t_1}}{k}\right] \qquad (5)$$

$$\frac{T_{w2} - T_i}{T_f - T_i} = 1 - exp\left[\frac{h^2 \alpha t_2}{k^2}\right] erfc\left[\frac{h\sqrt{\alpha t_2}}{k}\right] \qquad (6)$$

In this case, a transient infrared thermograph technique will be used to obtain both h and η from a single test, as described by Ekkad et al [17]. Thus, two images with surface temperature distributions are captured at two different times during the transient test.

A net heat flux ratio is used to measure the combined effect of film effectiveness and heat transfer coefficient Ekkad and Zapata [18]:

$$\frac{q''}{q_o''} = \frac{h}{h_o}\left(1 - \frac{\eta}{\emptyset}\right) \qquad (7)$$

The value for the overall cooling effectiveness (ø) ranges between 0.5 and 0.7.A typical value is Ø = 0.6, and this in general assumed in the present experimental analysis.

The IR images for models surface at each investigated test was captured and stored by a thermal camera. These images are transferred to the PC. Smart View Software program supplied with camera can be used to limit the selected area to avoid the effect of the test section walls. The IR images converted to corresponding temperature digital values and then saved as data in Excel sheet.MATLAB Software programs are prepared using a semi-infinite solid assumption to introduce the film cooling effectiveness and heat transfer coefficient contours. Equations, (4), (5), (6), and (7) was solved using MATLAB Software, Smart View Software, and Excel Software.

The measurement uncertainty was determined by using the methodology described by Holman and Bhattacharyya [16]. Error estimates for each variable are as follows: wall temperature ΔT_w = ±2 ºC, initial temperature ΔT_i = ±2 ºC, mainstream temperature ΔT_m = ±0.2 ºC, and coolant temperature ΔT_c = ±0.2 ºC. The camera frame rate is 60 Hz resulting in a time error Δt =±0.125 sec. and the test surface properties (α and k) uncertainty are taken from tabulated values, as a custom, 3% relative uncertainty is assumed for both variables. The resulting average uncertainty for heat transfer coefficient and film effectiveness is ±8.2% and ±11.0%, respectively.

3- Results and Discussions

Figures (3 to 5) show the effect of hole space ratios (S/D) on the temperature distribution for different blowing ratios (BR= 0.5, 1.0, and 1.5). Comparison between model 1, model 2 and model 3 showed that the model 1 gave high protection than the model 2 also model 2 give high protection than model 3, for the three blowing ratios. Also the figures 3 to 5 show that the coolant temperature distribution decreases as the blowing ratio increases for all the three models. The reason is that for a low momentum ratio (i. e. BR=0.5), the mainstream flow close to the test surface, the jet streamlines seems to go towards the surface and the

mainstream flow depart upward, therefore the mainstream push the jet towards the surface, and the interaction forms a low temperature film layer near the wall and give high protection effect, while for a high momentum ratio (i. e. BR=1.5), coolant jets have enough momentum to penetrate in to the cross mainstream. These results agree well with the results obtained by Sun et al. [19].

Figure (6) presents the span wise averaged film effectiveness (η_{sa}). (η_{sa}) is calculated as the average values taken from the local reading of 46 pixels in span wise direction in eighteen streamlines location downstream from the hole exist. Figures 4.4.a, 4.4.b and 4.4.c show that the model 1 gave high values of η_{sa} as compared to the two other models (model 2 and model 3). The overall average film cooling effectiveness (η_{av}) was calculated from the values of local film cooling effectiveness (η) for all the entire pixels values.

Figure (7) shows the effect of blowing ratio on η_{av} for the three models. This figure shows clearly that the values of η_{av} for the model 1 are higher than the other two models. It appears also that the values of η_{av} decreases as the blowing ratio increases for all the three models.

As a matter of fact, the enhancement of the blade surface protection is done by keeping the local heat transfer coefficient (h) as low as possible. The local heat transfer coefficients are calculated from the data of two IR images taken in successive times as described above. The average of the local heat transfer coefficient ratios (h / ho), in which (h and ho) represent the heat transfer coefficient on the plate surface with and without film cooling respectively are presented in Figure (8). The values of the average heat transfer coefficient ratio for the model 1 are higher than that the two other models for all blowing ratios and (h/ho) is increased with increasing the blowing ratio. The increment of (h/ho) is due to that the jet injection produces high turbulence level inside the mixing region.

In the practical application, turbine designers are concerned with the reduction of heat load to the film protected surface. The heat load can be presented by combining film cooling effectiveness (η) and the heat transfer coefficient ratio (h/ho), according to equation (7), therefore the ratio (q/qo) can be calculated. (q/qo) represent the reduction in heat flux at the tested surface with the presence of coolant air. If the values of these ratios are less than 1, then the film coolant is beneficial according to Lu et al.[20], while if the values are greater than 1, therefore effect of the film coolant is poor.

Figure (9) shows the effect of the blowing ratio on the overall heat flux ratios (q/qo). It is clear that from this Figure the model 1 provides significant reduction of heat flux at all tested BR than that of the other models.

4- Conclusion

The present work has reached to the following conclusions:

1- The thermal performance decreases as the span ratio (S/D) increases for all blowing ratios.

2- The film cooling effectiveness decreases as the blowing ratio increases for all the three models.

3- The values of the average heat transfer coefficient ratio (h/ho) for the model 1 are higher than that the two other models for all blowing ratios and (h/ho) is increased with increasing the blowing ratio.

Nomenclatures

D	Hole diameter	m
h	Heat transfer coefficient with film cooling	$W/m^2 \cdot K$
h_o	Heat transfer coefficient without film cooling	$W/m^2 \cdot K$
k	Thermal conductivity	$W/m^2 \cdot K$
S	Span wise hole spacing	m
t	time	s
T	Temperature	℃
T_c	Coolant temperature	℃
Ti	Initial temperature	℃
T_m	Hot mainstream temperature	℃
T_w	Wall temperature	℃
U_c	Coolant velocity	m/s
U_m	Hot mainstream velocity	m/s
η	Film cooling effectiveness	-
η_{av}	Average film cooling effectiveness	-
η_{sa}	Stream wise Average film cooling effectiveness	-
ρ	Density of air	kg/m^3
ρ_c	Density of coolant air	kg/m^3
ρ_m	Density of hot mainstream	kg/m^3
θ	Inclination angle	Degree

References

[1]. Benabed, M., Azzi A., and Jubran, B.A., 2010, "Numerical investigation of the influence of incidence angle on asymmetrical turbine blade model showerhead film cooling effectiveness", Heat Mass Transfer, Vol. 46, PP. 811-819.

[2]. Han, J.C. and Ekkad, S.V., " Recent Development in Turbine Blade Film Cooling", International Journal of Rotating Machinery, Malaysia, Vol. 7, No. 1, 2001, pp. 21-40.

[3]. Han, J.C., Dutta, S. and Ekkad, S., 2000, "Gas Turbine Heat Transfer and Cooling Technology", Taylor and Francis, New York, pp. 129-136.

[4]. Bunker, R.S., 2009, "Film Cooling: Breaking the Limits of Diffusion Shaped Holes", Proceeding of International Symposium on Heat Transfer in Gas Turbine, Antalya, Turkey.

[5]. Ahn, J., Jung, I.S., and Lee, J.S., "Film cooling from two rows of holes with opposite behavior and adiabatic film cooling effectiveness", International Journal of Heat and Fluid Flow, Vol. 24, 2003, pp. 91-99.

[6]. Han, J.C. and Rallabandi, A. P.,2010, "Turbine Blade Film Cooling Using PSP Technique", Frontiers in Heat and Mass Transfer, Texas, 77843-3123, USA.

[7]. Andrews, G.E., Khalifa, I.M., Asere, A.A., and Bazdidi-Tehrani, F. 1995," Full Coverage Discrete Hole Film Cooling: The Influence of Hole Size", ASME 85-GT-47.

[8]. Andrews, G.E., Asere, A.A., Gupta, M.L., and Mkpadi, M.C., 1985," Full Coverage Effusion Film Cooling with Inclined Multihole Walls with Different Hole Arrangements", ASME GT2003-38881.

[9]. Lu, Y.,Dhungel, A.,Ekkad, S.V., and Bunker, R.S., 2007, "Effect of Trench Width and Depth on Film Cooling from Cylindrical Holes Embedded in Trenches", ASME Paper GT 2007-27388.

[10]. Lu, Y., Dhungel, A., Ekkad, S.V., and Bunker, R.S., 2007, "Film Cooling Measurements for Cratered Cylindrical Inclined Holes", ASME Paper GT 2007-27386.

[11]. Martiny, M., Schulz, A., and Witting, S. 1995," Full coverage Film Cooling Investigations Adiabatic Wall Temperature and Flow Visualization", ASME 95-WA/HT-4.

[12]. Gustafsson, K.M., and Johansson, T., 2001, " An experimental Study of Surface Temperature Distribution on Effusion- Cooled Plates", Journal of Engineering for Gas Turbines and Power Transactions of the ASME 123(2001) 308-316.

[13]. Ekkad, S.V., Shichman, O., and Bunker, R.S., 2004, "Transient Infrared Thermography Method for Simultaneous Film Cooling Effectiveness and Heat Transfer Coefficient Measurement from a Single Test", Journal of Turbomachinery Transactions of the ASME 126(2004) 597-603.

[14]. Dhungel, A., Phillips, A., Ekkad, S.V., and Heidmann, J.D., 2007, "Experimental Investigation of a Novel Anti-Vortex Film Cooling Hole Design", ASME IGTI Turbo Expo, Montreal, Paper GT 2007-27419.

[15]. Alwan, M.Sh., 2012," Experimental and Numerical Investigation of Film Cooling Thermal Performance for Staggered Rows of Circular Jet", PhD Thesis, Mechanical Engineering Department , University of Technology.

[16]. Holman, J.P. and Bhattacharyya, S., "Heat Transfer", Ninth Edition, New Delhi, McGraw-Hill, 2008.

[17]. Ekkad, S.V., Ou, S., and Rivir, R.V., "A Transient Infrared Thermography Method for Simultaneous Film Cooling Effectiveness and Heat Transfer Coefficient Measurements from a single test", GT 2004-54236, Proceedings of ASME Turbo Expo 2004, Vienna, Austria.

[18]. Ekkad, S.V., and Zapata, D., "Heat transfer coefficients Over a Flat Surface with Air and CO2 Injection Through Compound Angle Holes Using a Transient Liquid Crystal Image Method", ASME Journal of Turbomachinery Vol. 119, No. 3, 1997, pp. 580-586.

[19]. Sun, W., Chao, J.H., Chen, Y.W., and Miao, J.M., 2009, "Numerical study on the Effusion Cooling Performance over the Walls of an Annular Burner", Seventh International Conference on CFD in the Minerals and Industries CSIRO, Melbourne, Australia.

[20]. Lu, Y., Dhungel, A., Ekkad, S.V., and Bunker, R.S., 2007, "Film cooling measurements for cratered cylindrical inclined holes", ASME Paper GT 2007-27386.

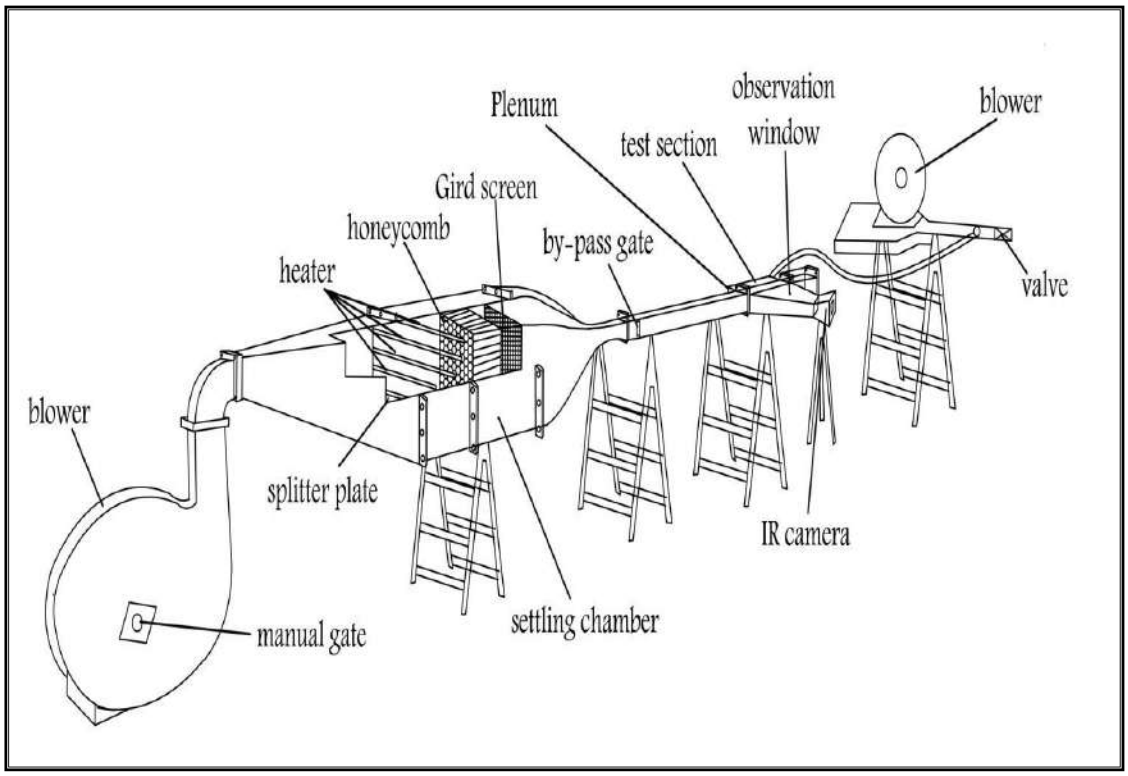

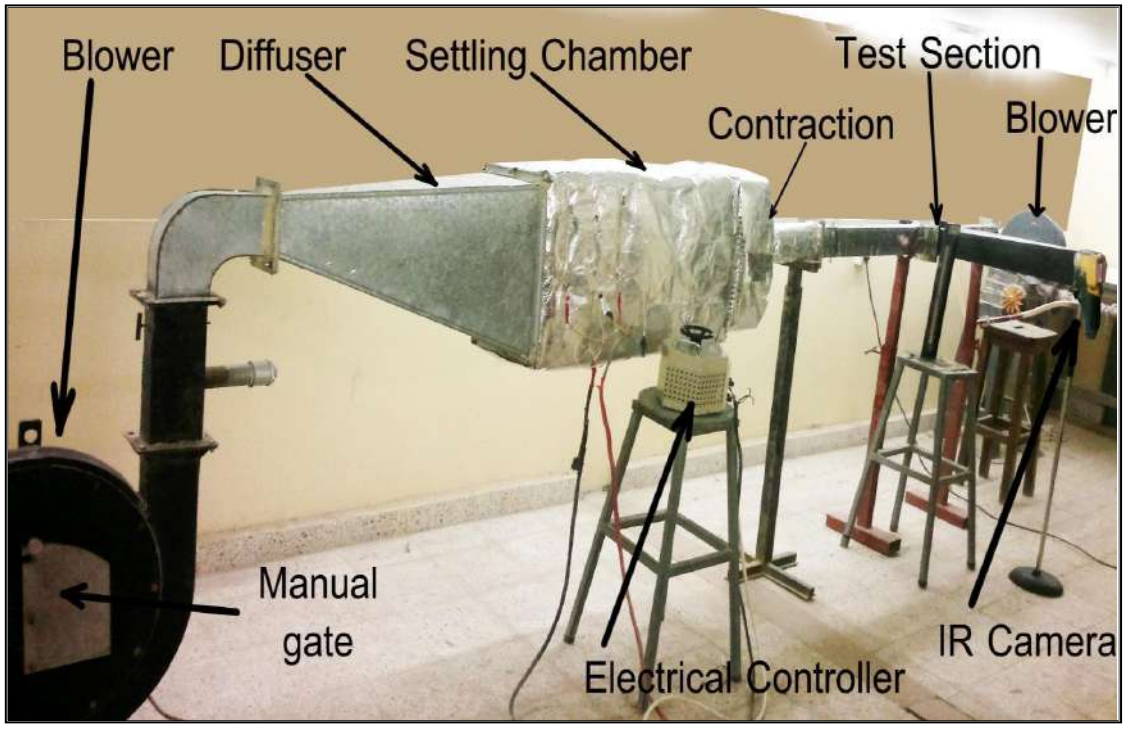

Figure (1) Schematic and photography of the test rig

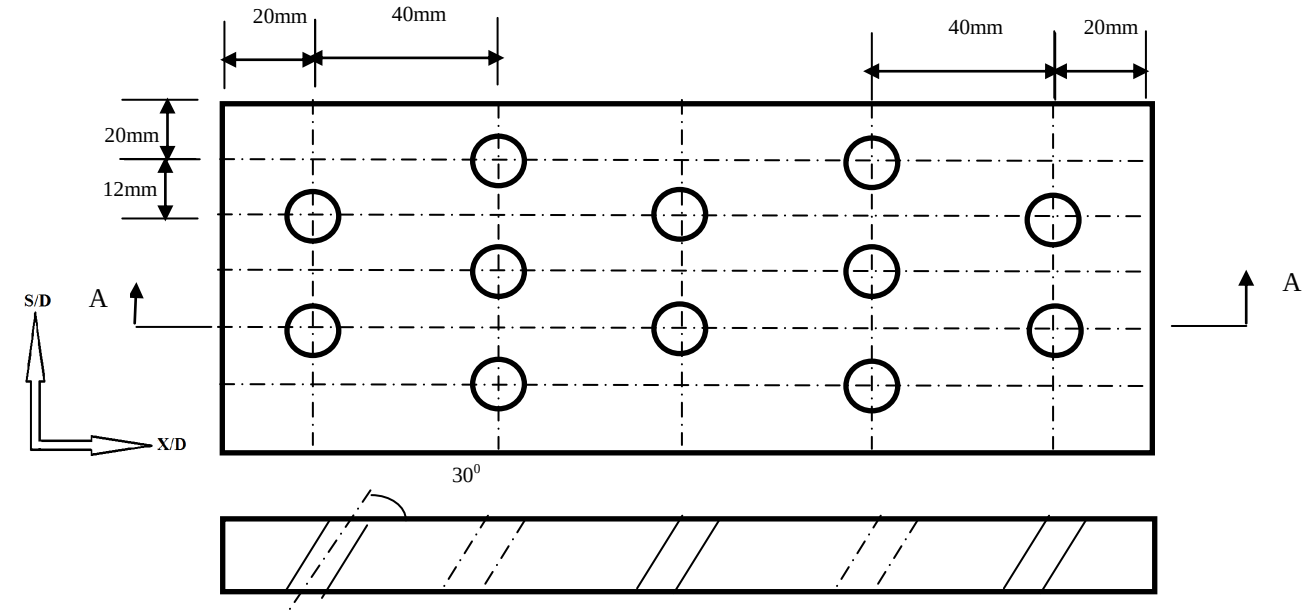

(a) X/D= 10, S/D = 3

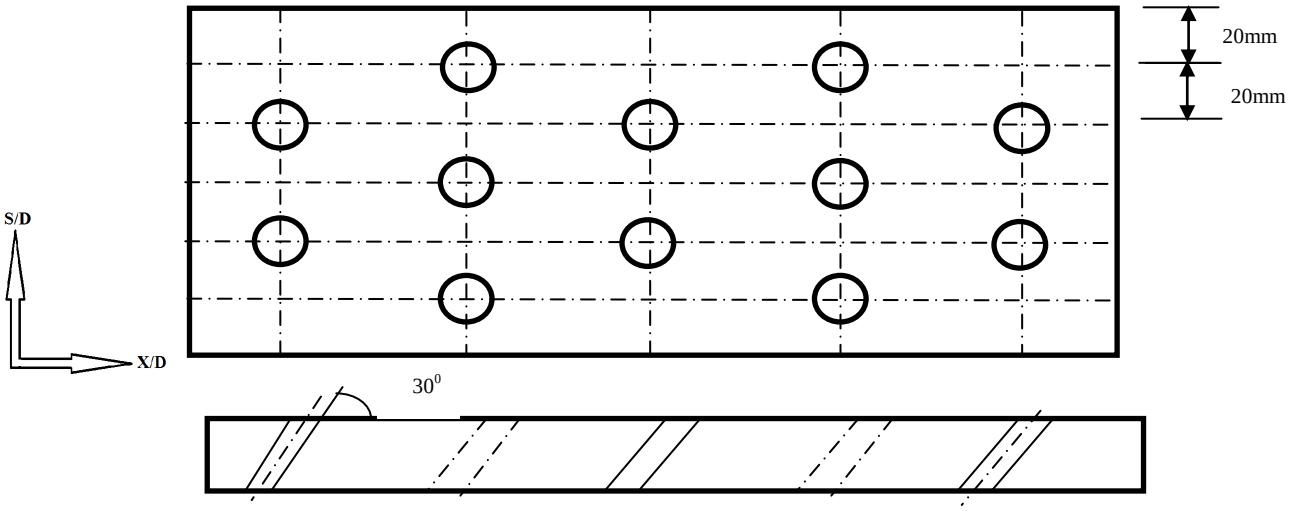

(b) X/D= 10, S/D = 5

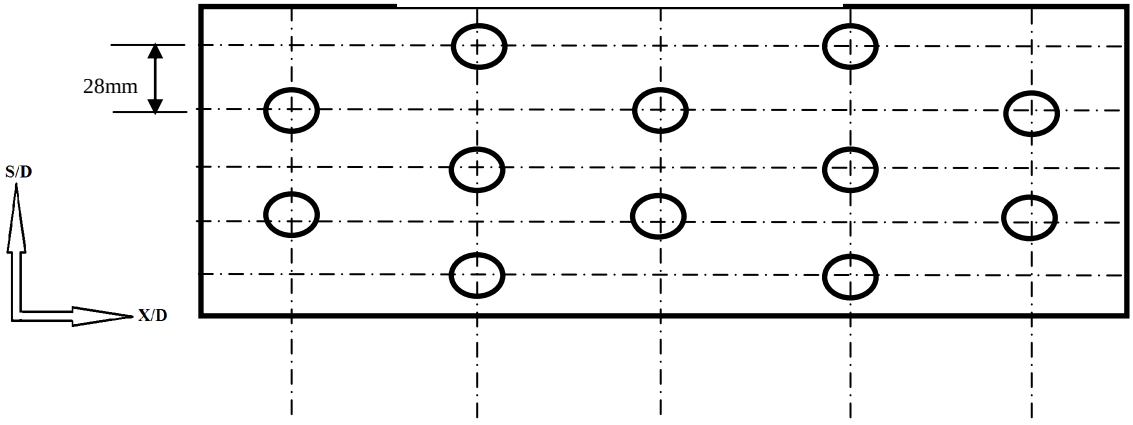

(c) X/D = 10, S/D = 7

Figure (2) Details of three test models : (a) X/D= 10, S/D = 3 & (b) X/D = 10, S/D = 5& (c) X/D= 10, S/D = 7

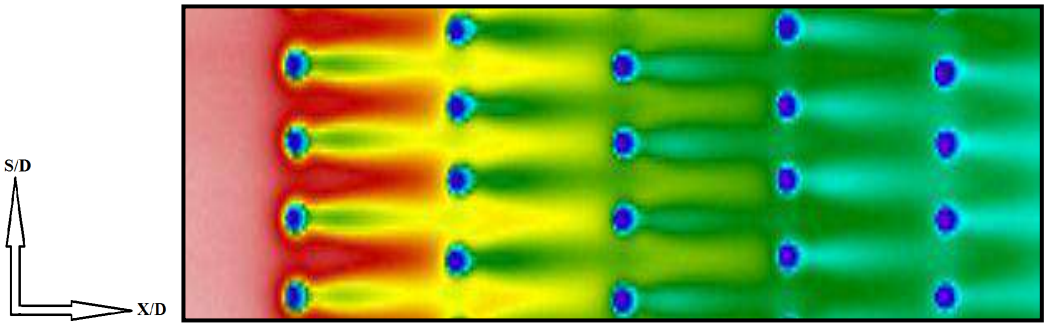

BR=0.5

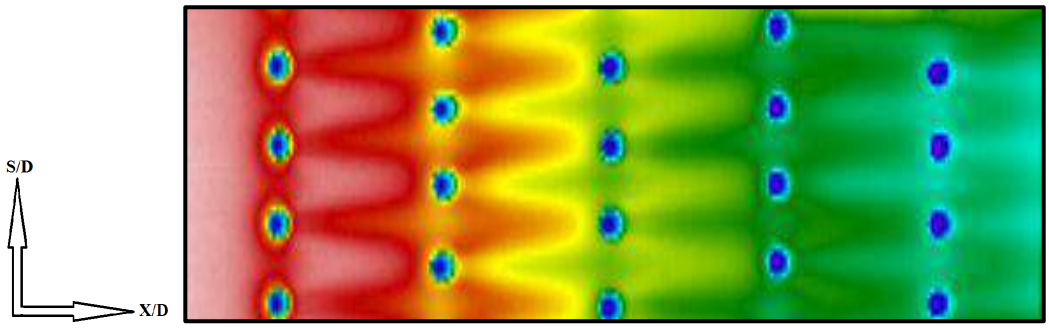

BR=1.0

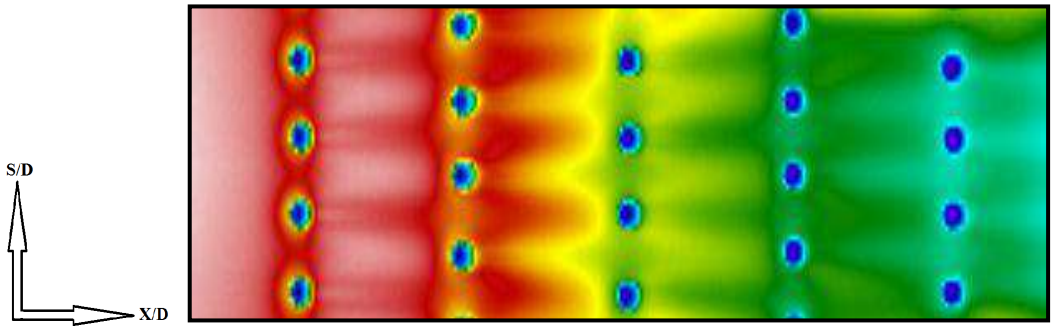

BR=1.5

Figure (3) Contours of temperature distribution for model 1 (X/D=10 & (S/D=3) at different blowing.

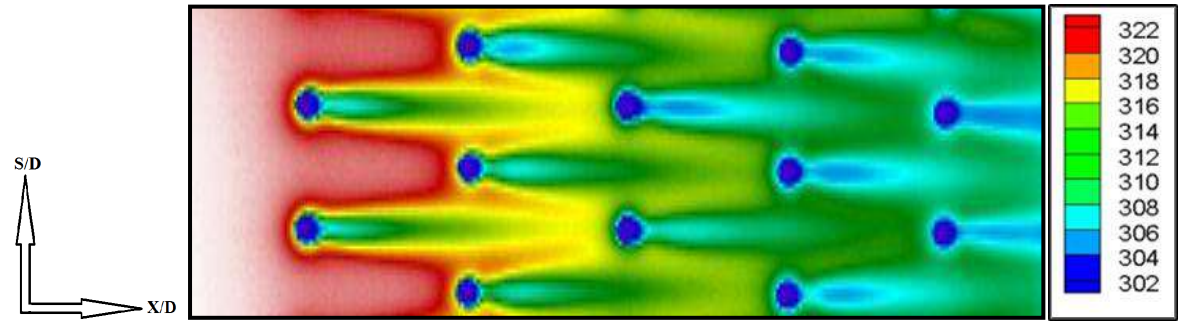

BR=0.5

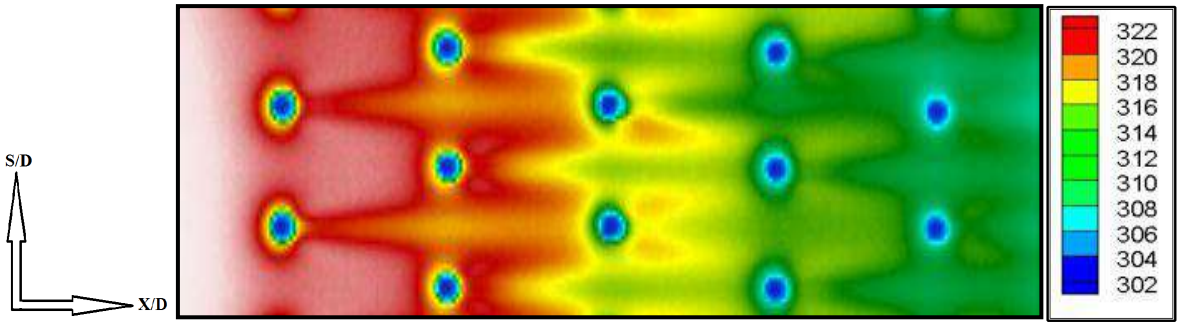

BR=1.0

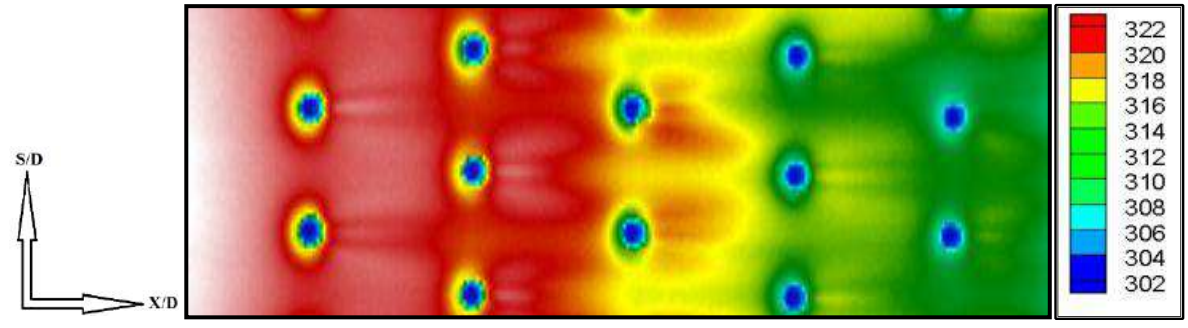

BR=1.5

Figure (4) Contours of temperature distribution for model 2 (X/D=10 & S/D=5) at different blowing.

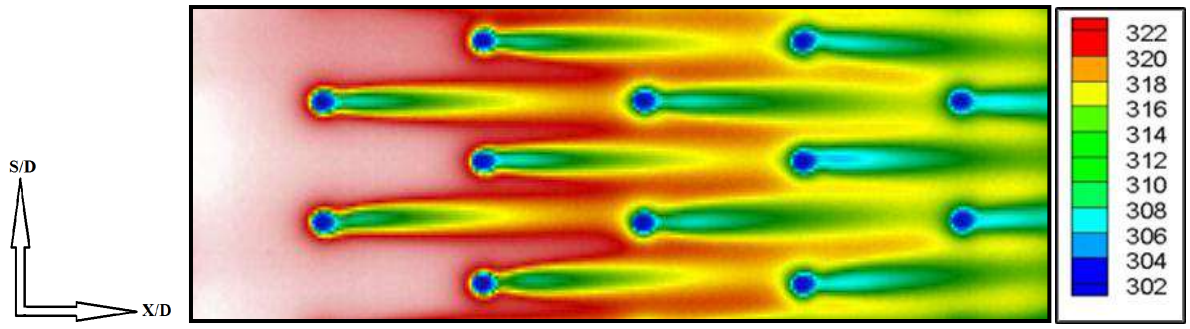

BR=0.5

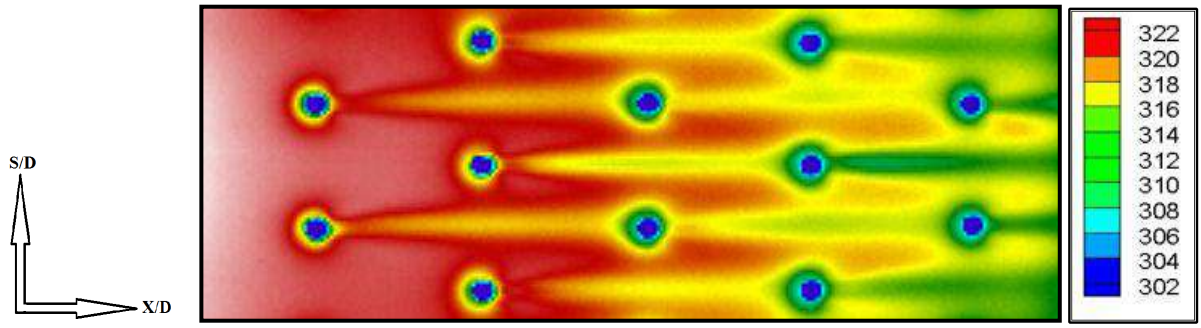

BR=1.0

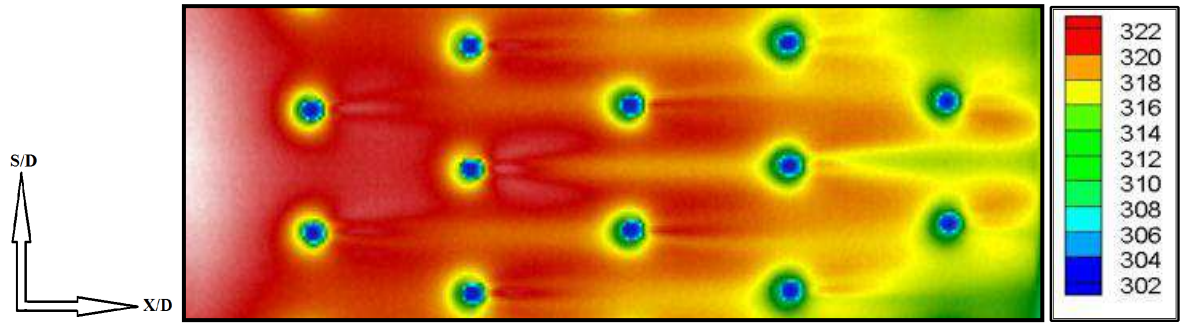

BR=1.5

Figure (5) Contours of temperature distribution for model 3 (X/D=10 & S/D=7) at different blowing ratio.

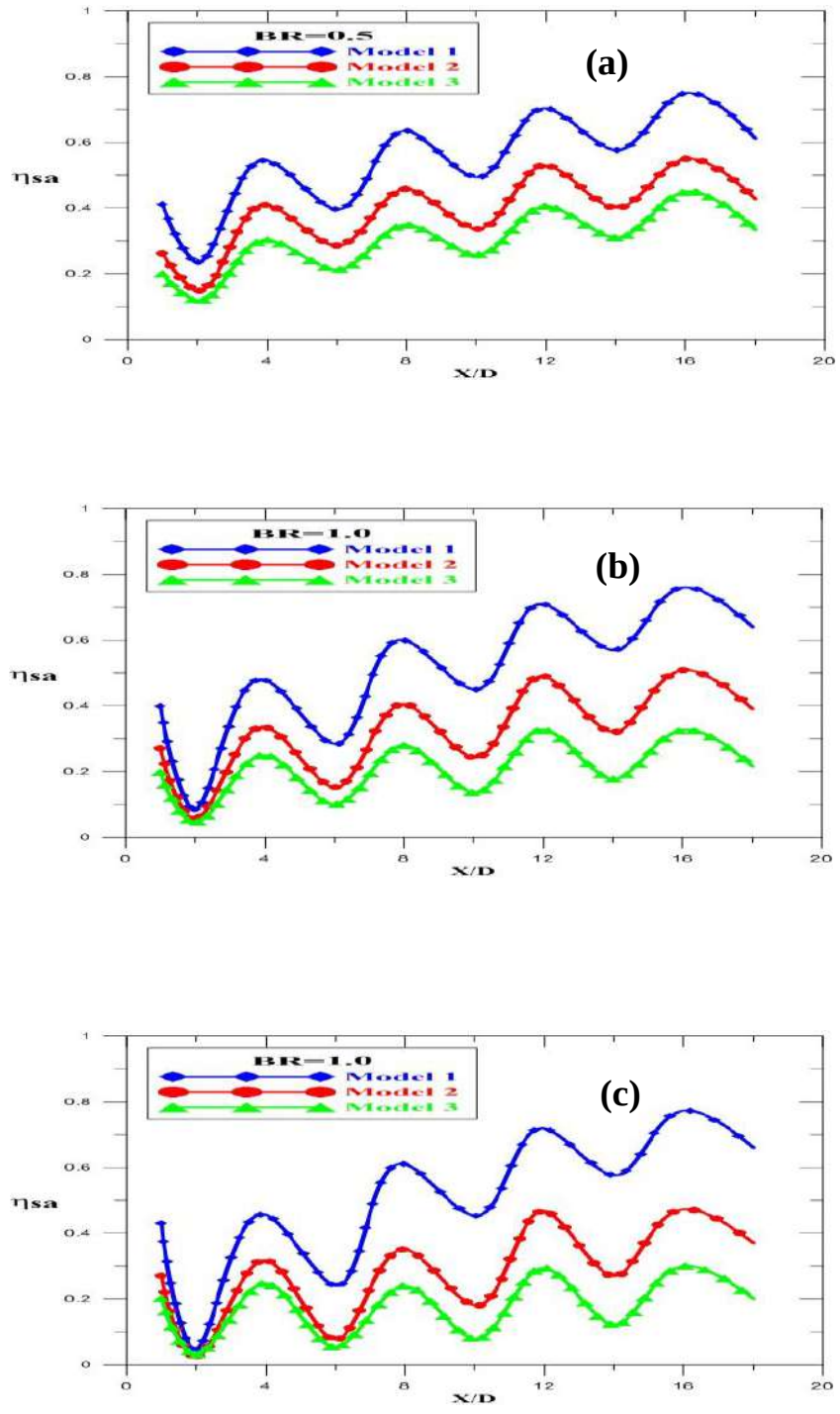

Figure (6) Effect of row spacing (S/D) on span wise averaged film cooling effectiveness at: (a) BR=0.5, (b) BR=1.0, (c) BR=1.5.

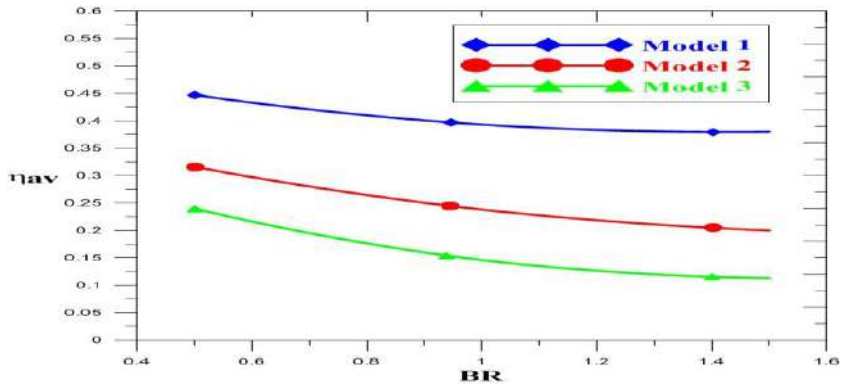

Figure (7) Effect of blowing ratio on averaged film cooling effectiveness for models (1, 2 and 3).

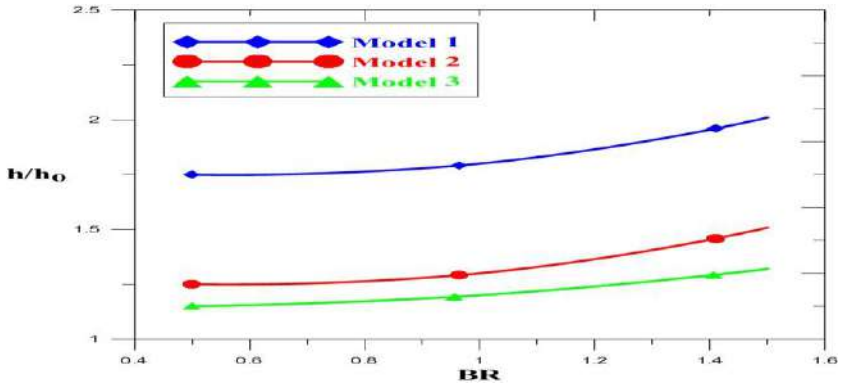

Figure (8) Effect of blowing ratio on averaged heat transfer coefficient for models (1, 2 and 3).

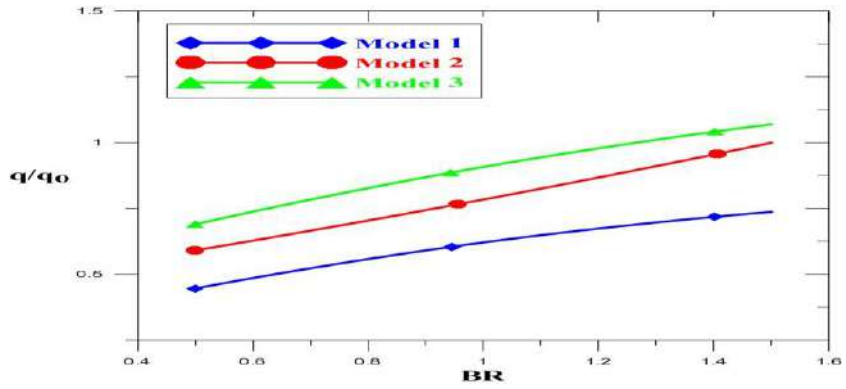

Figure (9) Effect of blowing ratio on overall heat flux ratio for models (1, 2 and 3).